ADVANCED FUNCTIONAL MATERIALS
www.afm-journal.de

Autonomous Self-Sustained Liquid Crystal Actuators Enabling Active Photonic Applications

Ren Zheng, Lingling Ma, Wei Feng, Jintao Pan, Zeyu Wang, Zhaoxian Chen, Yiheng Zhang, Chaoyi Li, Peng Chen, Hari Krishna Bisoyi, Bingxiang Li,* Quan Li,* and Yanqing Lu**

Advances in biomimicry have led to the rise of advanced robotics, posing promising revolutions across a variety of fields. Programmable self-sustained actuation in nature, such as human's heart beating, bird's wingbeats, and penguin's waddling, are intriguing and inspiring but challenging for device innovation, which hinders the emergence of autonomous self-feedback applications, especially in optics and photonics. Herein, the design, fabrication, and operation of crosslinked liquid crystal actuators are described that combine the programming of microstructures and the engineering of macroscopic shape morphing for active optics and photonics. The actuators consist of twisted nematic liquid crystal molecules with both elastic and optical anisotropies, resulting in large bending deformations in response to heat. Programmable bending motions and self-sustained waddling oscillations are demonstrated, further contributing to the achievements of dynamic 2D beam steering and self-sustained light field modulation. It is envisioned that these actuators with self-sustained performances without requiring turning the stimulus on-off will find applications in autonomous active optical systems, photonic applications, as well as self-governing robotics with the core feature of thermo-mechanical-optical transduction.

1. Introduction

Nature has long been considered a source of inspiration in developing artificial materials/devices with adaptation and intelligence in response to external stimuli.[1] Prime examples include *Mimosa pudica*, sunflower, and chameleon, triggering the inventions of nanomedicine strategies,[2] flexible solar trackers,[3] color-changing soft robotics,[4] and so on. Another class of stimuli-responsive actuation with autonomous, self-sustaining features is also ubiquitous in living organisms, playing important roles in various life activities.[5] For instance, penguins adopt a waddling gait, periodically swinging to the left and right, reminiscent of tumblers.[6] Such waddling gait was reported to smartly decrease the muscular work by maximally exchanging the gravitational potential and kinetic energies, conserving 80% mechanical energy within each step.[6] Many other examples include fishtailing, heart beating, and wingbeats.[7] Wang et al.[8] reported a self-governing thermo-mechanoelectrical system for multimodal locomotion and electricity generation. Although much effort has been made to develop responsive actuators relying on on-off or regulations of the external stimuli by soft materials,[9] it is still challenging to achieve programmable self-initiated, self-feedback, and self-sustained actuation with a versatile material system exploitable for specific optical applications.[8,10]

R. Zheng, L. Ma, J. Pan, Z. Wang, Z. Chen, Y. Zhang, C. Li, P. Chen, Y. Lu
National Laboratory of Solid State Microstructures
Key Laboratory of Intelligent Optical Sensing and Manipulation
College of Engineering and Applied Sciences
Collaborative Innovation Center of Advanced Microstructures
Nanjing University
Nanjing 210023, China
E-mail: malingling@nju.edu.cn; yqlu@nju.edu.cn

W. Feng
Physical Intelligence Department
Max Planck Institute for Intelligent Systems
70569 Stuttgart, Germany

H. K. Bisoyi, Q. Li
Advanced Materials and Liquid Crystal Institute and Materials Science Graduate Program
Kent State University
Kent, OH 44242, USA
E-mail: quanli3273@gmail.com

B. Li
College of Electronic and Optical Engineering & College of Flexible Electronics (Future Technology) Nanjing University of Posts and Telecommunications
Nanjing 210023, China
E-mail: bxli@njupt.edu.cn

Q. Li
Institute of Advanced Materials and School of Chemistry and Chemical Engineering
Southeast University
Nanjing 211189, China

The ORCID identification number(s) for the author(s) of this article can be found under https://doi.org/10.1002/adfm.202301142

DOI: 10.1002/adfm.202301142

The field of active photonics has undergone significant expansion in the last decade due to the rapid developments of optical communications, metaverse, and optical computing.[11] Among the broad family of optical materials, dynamically tunable liquid crystals (LCs)[12] are widely investigated as active materials in optoelectronic and photonic devices.[13] By employing polymerized LCs (such as LC elastomers and LC networks), which show excellent features of elastic deformability,[14] structural patterning,[15] multi-stimuli responsiveness,[16] and facile miniaturization,[17] various mechanical actuations including autonomous self-propelled motions have been demonstrated.[5a,d,18] For instance, Cunha et al.[19] reported the light-driven continuous oscillatory rocking of an LC polymer film with the mechanism of self-shadowing effect. Reversible swinging phenomena of the bionic dog swinging tail[20] and photoactive self-winding fiber actuators inspired by the helix formation of plant tendrils[5b] were also presented. Such autonomous actuations are all performed under constant stimulations without requiring turning on-off or changing the external fields,[5b,19–21] which are quite promising and vital for future intelligent optical techniques. However, due to the cross-scale research of microstructure-based optical effects and macroscale mechanical dynamics, difficulties also exist in leveraging the programmable, self-propelled, self-sustained mechanical actuation into unique optical and photonic functions. If one can incorporate the interactions between optical microstructure design and macroscopic shape morphing within polymerized LC films, diversified LC actuators (LCAs) would be anticipated, permitting autonomous, active, efficient, and even multimodal mechanical-optical functionalities.

Here, we devise bioinspired soft smart LCAs that can perform autonomous self-sustained actuation for active photonic applications (**Figure 1**a). The LCAs are tailored into ribbons with intrinsic twisted nematic structures to induce the asymmetric thermo-mechanical response. Programmable bending actuation and bioinspired self-sustained waddling motions coupling with built-in thermo-mechanical and mechano-thermal feedback loops are demonstrated by providing an appropriate thermal field. In addition, we achieve continuous and ceaseless thermo-mechanical-optical actuation based on elaborately microstructured LCAs, including programmable self-sustaining beam steering, optical switching, and special light field modulations, by continuously harvesting thermal energy from the external surroundings. This work not only takes advantage of the macroscopic designing of elastic anisotropy of LCAs but also combines the microscopic engineering of optical anisotropy of LCs for active optical and photonic applications. This seamless integration exceeds previous reports that usually only paid attention to the mechanical response of LC polymer films, thus it provides a new sight of smart actuators with distinctive functions of thermo-mechanical-optical transduction.

2. Results

2.1. Experimental Design

Polymerized LC film is an active optical and mechanical material system with the stimuli-mechanical responsiveness inherently encoded in its structure. To attain thermo-mechanical bending actuation, we design ribbon-like LCAs with a symmetry-breaking geometry of twisted nematic director configuration by introducing orthogonal alignment conditions to the upper and bottom surfaces of the film. When the ribbon is exposed to hot surfaces beyond its glass transition temperature (T_g = 42.8 °C, Figure S1a, Supporting Information), the in-built orientational order of LCs decreases, resulting in anisotropic shrinkages and expansions at the two surfaces (contraction along the LC director and the elongation in the orthogonal direction). Consequently, macroscopic bending deformations are obtained with a lifted center of gravity of LCAs (Figure 1a). The continuous increase in temperature makes the height of the center of gravity surpass a certain threshold. Then, the LCA senses subtle perturbation that triggers the initiation of unrelenting self-sustained oscillations

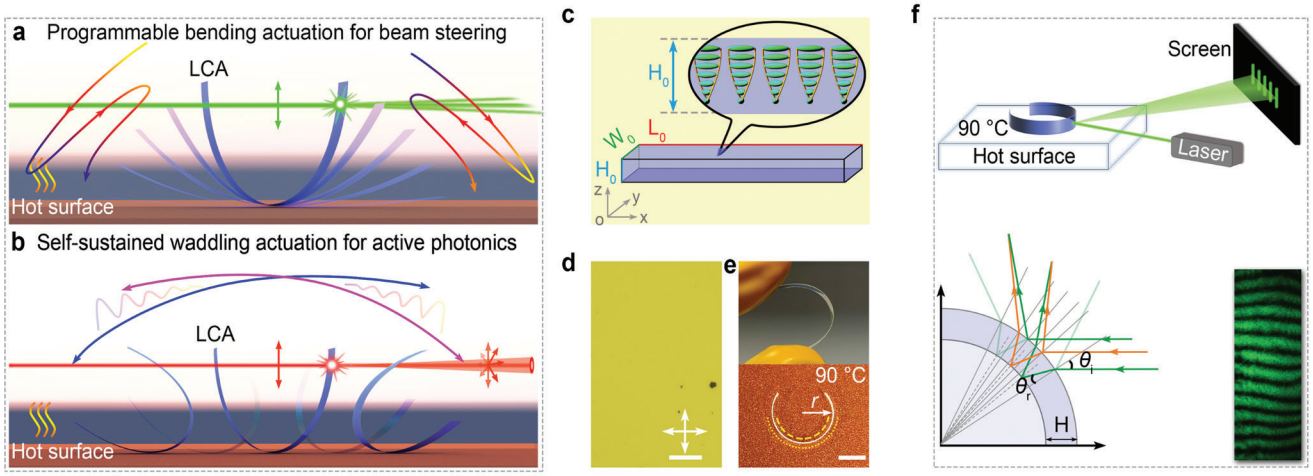

Figure 1. Characterizations of LCA films. a,b) Schematic concept of programmable bending actuation and self-sustained waddling actuation for dynamic optical applications. c) Schematic illustration of an LC ribbon with the twisted orientation of LC directors. L_0, W_0, and H_0 represent the length, width, and thickness of the LC ribbon, respectively. d) POM texture of the LC ribbon viewed between crossed polarizers. Scale bar: 100 μm. e) Stress-induced (top) and thermal-induced (bottom) curved LC ribbons. The curvature of the film at 90 °C is 1.9 cm^{-1}. Scale bar: 5 mm. f) Schematic of the reflected thin-film interference and reflected interference fringes. The wavelength of the incident laser beam is 532 nm.

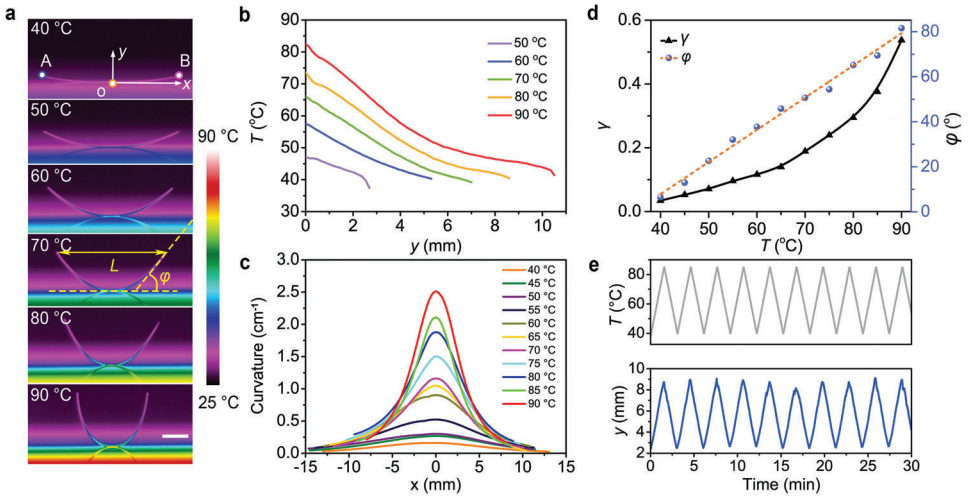

Figure 2. Programmable bending actuation of LCAs. a) Infrared images of bending LCAs at different temperatures. Scale bar: 5 mm. b) Temperature distribution of LCA on the hot surface with different temperatures. c) Curvature distribution of LCA at different temperatures. d) Factors of γ and φ changing with the setting temperature. e) Programmable bending deformation at sequentially changed temperature.

reminiscent of the penguins' waddling gait (Figure 1b). We further pose the programmable autonomous optical/photonic performances by taking advantage of the light field modulation ability of LC microstructures, with the core feature of thermo-mechanical-optical transduction.

The materials and fabrications of LCAs are provided in Text S1 and Figures S1b and S2–S5 (Supporting Information). LCA with twisted nematic structure (Figures 1c), high optical transparency, and good mechanical flexibility reveals generally uniform textures under both the dark-field metalloscope and crossed polarized optical microscope (POM, Figure 1d,e; Figures S6 and S7, Supporting Information). The XRD characterization of the LCA is also carried out (Figure S8, Supporting Information), showing an absence of layer reflections and a diffuse reflection in the wide-angle region (half-peak width $w = 7.7°$), supporting the assignment of twisted nematic structure. LCA can agilely respond to a thermal field by spontaneously bending in a coiling manner when laterally laid on a hot surface ($T = 90$ °C, Figure 1e). We take an optical interferometry method to detect the deformation in the transverse direction of the LCA. As shown in Figure 1f and Figure S9 (Supporting Information), a linearly polarized laser beam with a spot diameter of 1.5 mm strikes the curled LCA at the incident angle of 35°, which is partly reflected and partly refracted, with the refracted portion further split into higher-order refracted waves through internal reflections. Hence, thin-film division-of-amplitude interference with slightly curved interference fringes is observed, verifying the saddle-like form of frustration. Such deformations are reversible when the temperature decreases to room temperature (26 °C), suggesting a reliable reconfigurable actuation.

2.2. Programmable Bending Actuation

The thermo-mechanical performances of the LCA are studied to test the response to heat stimuli. A flat ribbon-like LCA with $W_0 = 2$ mm is placed on the surface with its upper surface possessing LC directors parallel to the longitudinal direction (LCAs with other widths are described in Text S2 and Figure S10, Supporting Information). As shown in **Figure 2**a and Figure S11 (Supporting Information), while the temperature T of the hot surface increases from 40 to 90 °C, the LCA successfully converts thermal energy into kinetic energy. The overall structure bends upward, and the two arms of the LCA are gradually lifted due to the thermally induced asymmetric internal strain. Notably, a slight vibration is observed at two endpoints A and B of the LCA when $T = 90$ °C and the elevated film parts cool down rapidly as they are away from the hot surface, which recover to flat forms facilitating the optical performance when introduced elaborate microstructures. A slight difference between the measured temperature from infrared images and the actual temperature of the film is explained in Text S3 (Supporting Information) with Figures S12 and S13 (Supporting Information).

Figure 2b,c manifest different curvature profiles of LCA and changes in temperature distribution along the length direction of the ribbon at different setting temperatures. Typically, from the middle of the film (point o) in contact with the hot surface to point A or B, the temperature of LCA continuously attenuates from the maxima. The temperatures at ends of the LCA are always ≈40 °C at different setting temperatures, which is because these parts of the film are beyond regions of vertical temperature gradient and the heat transfer takes place with the same surrounding atmospheres (≈26°C). The maximum bending curvature exists at point o, which increases to 2.5 cm^{-1} as $T = 90$ °C, larger than that reported in previous research with twisted nematic configuration.[22] In addition, factors γ and φ are introduced to quantitatively analyze the thermal responsiveness of the films, where γ is defined as $(L_0\text{-}L)/L_0$ and the bending degree φ denotes the angle between the asymptotes of the right arm of LCA and the horizontal line (Figure 2a). As shown in Figure 2d, γ is significantly increased with the increasing T, $\gamma = 0.54$ at $T = 90$ °C. The increase of φ is almost linear with T with the slope of 1.4.

Programmable thermo-mechanical bending actuation of LCA is further investigated by engineering the heating and cooling

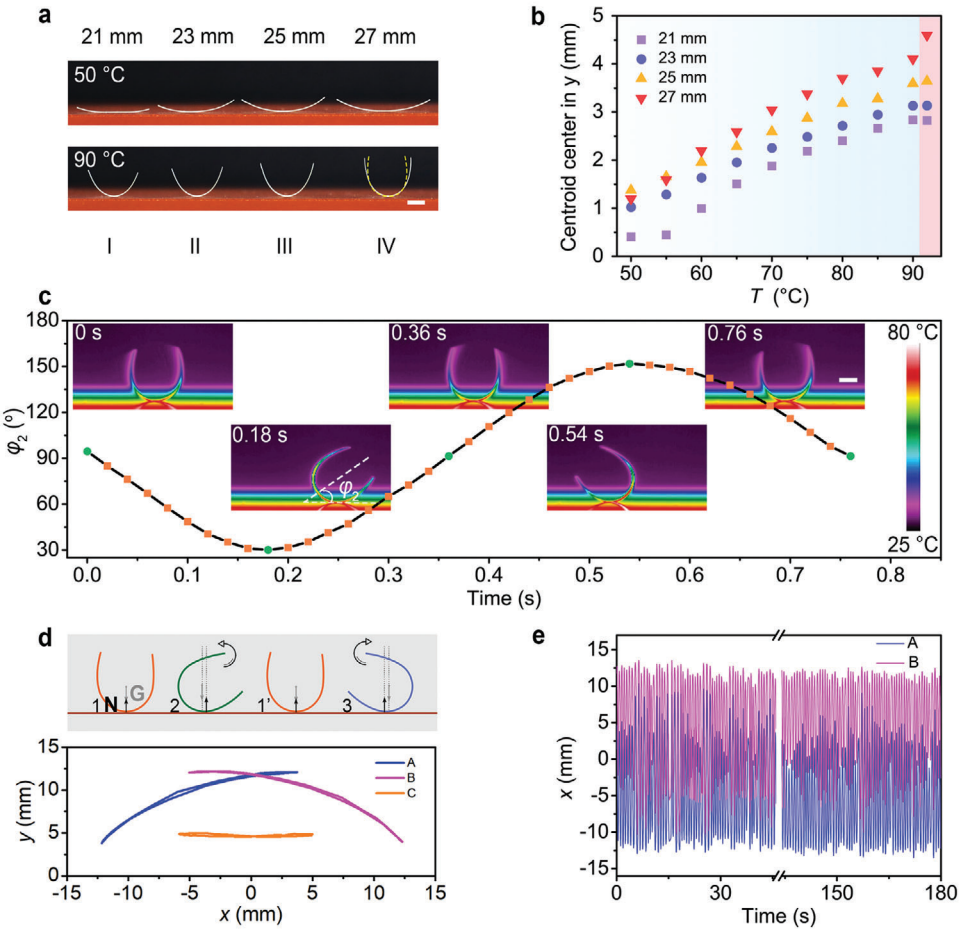

Figure 3. Bioinspired self-sustained waddling oscillations of LCAs. a) Photos of curved LCAs with varied lengths (L_0 = 21 mm, 23 mm, 25 mm, and 27 mm) and the same W_0 = 2 mm. T = 50 °C (top); T = 90 °C (bottom). The dashed yellow line indicates the shape morphing of LCA IV at T = 92 °C. The temperature for the initiation of tumbling of LCA III is ≈105 °C. Scale bar: 5 mm. b) Relationship between the height of centroid center and T. c) Time-dependent change of φ_2 and corresponding infrared images of LCA during the self-sustained waddling motion. φ_2 denotes the angle between the axis of symmetry of LCA and the horizontal line. Scale bar: 5 mm. d) Schematic diagram of the mechanism of waddling actuation (top); 2D trajectory of endpoints (A, B) and the centroid center (C) in the x-axis during a waddling cycle (bottom). e) Time-dependent motion of points A and B in the x-axis.

processes. We adopt a temperature controller by setting the temperature range (40 °C – 85 °C), the changing rate (30 °C min^{-1}), and the number of heating/cooling cycles (>10) to achieve the cyclical actuation. Two arms of the LCA exhibit a periodically flapping motion with the height (y) of the endpoint B varying (in the range of 2.4 mm to 8.9 mm) synchronously with the changing of T (Figure 2e; Movie S1, Supporting Information). Moreover, an LC athlete with programmable sit-up actuation is further investigated (Figure S14, Supporting Information). It can sit up quickly when the temperature rises to 90 °C, and returns to a flat gesture vividly when T is gradually reduced to ≈40 °C, indicating a good recoverability (Movies S2 and S3, Supporting Information).

2.3. Autonomous Self-Sustained Waddling Actuation

We explore the capability of bioinspired self-governing waddling actuation of LCAs by further increasing the temperature. First, we break the equilibrium of LCA by continuously lifting its center of mass to initiate the waddling. As shown in **Figure 3**a, centroid centers of different-sized LCAs are examined. The length of LCAs I, II, III, and IV are 21 mm, 23 mm, 25 mm, and 27 mm (W_0 = 2 mm), respectively. LC directors parallel to the longer side of the ribbon are facing upwards. With the temperature increases from 50 to 90 °C, LCAs bend and the contact areas between the ribbons and the hot surface become smaller, increasing the instability (Figure S15, Supporting Information). Their centroid center shifts in y exhibit nearly linear increase trends (Figure 3b, see the definition of centroid center in Text S4, Supporting Information). Once the surface temperature reaches 90 °C, we observe a discontinuous, irregular, weak motion of LCA IV with its endpoints A and B vibrating slightly while other LC ribbons remain in static states. Further increase in temperature (92 °C) triggers the tumble of LCA IV falling to one side (Movie S4, Supporting Information). Then, the original symmetric temperature distribution of the LC ribbon is broken by leveraging the rapid regional heat transfer among the hot surface, the LCA, and the air, which initiates the autonomous self-sustained waddling actuation. An abruptly higher centroid center of C_y = 4.6 mm is found at 92 °C (Figure 3b) owing to the obvious shape difference

resulted from the dynamic heat flow and heat-flow-induced instantaneous bending and recovery. γ exceeds 0.6 at $T = 92$ °C comparable with that reported in previous research.[5a,8,23]

A complete self-sustained oscillatory actuation from the neutral to the rightmost, leftmost, and then back to the neutral position, along with the time-dependent change of φ_2, is presented in Figure 3c and Figure S16 (Supporting Information) ($T = 92$ °C). Detailed investigation shows LCAs undergo a fast bending deformation within 3.6 s before actuating the continuous oscillatory behavior (Figure S17 and Movie S5, Supporting Information). Then the oscillation amplitude quickly maximizes in the following 1.0 s and stays constant after that. During the shift of the center of gravity, the LCA maintains a barely variant macroscopic bending curvature profile, facilitating a non-fatigue enduring activity. The change of heat distribution is similar to the water flow within an oscillatory U-shaped tube, establishing unique self-locked thermo-mechanical and mechanical-thermal feedback loops for autonomous oscillation (Movie S6, Supporting Information). The oscillation trajectory and amplitude of endpoints as well as the centroid position of LCA are plotted in Figure 3d,e, exhibiting a symmetrical translational waddling motion. The average oscillation amplitude of centroid center in the *x*-axis is 10.8 mm (Figure S18, Supporting Information) and the oscillation frequency is 1.3 Hz. We monitored the motility of LCAs at 92 °C for tens of minutes (Movie S7, Supporting Information), revealing ceaseless autonomous waddling oscillations unless an accidence due to unexpected external disturbances.

Based on these findings, we propose a mechanism for the waddling actuation of the LCA base on the dynamic thermo-mechanical behavior and general principle of a lever (Figure 3d, top). In the initial state, the film is subjected to two forces, i.e., the gravity and the bracing force, with the same *x*-axis of force bearing points and equal magnitudes in opposite directions (state_1). When the equilibrium of the LCA is broken, waddling oscillation is initiated with the film rocking to one side. As a result, the force bearing point of bracing force shifts to the right of the gravity force after it reaches the rightmost position (state_2), which produces a left-rotation force moment to make the LCA stop and tend to right itself. An additional contribution to the same backwards waddling motion is the cooling of the left arm of LCA away from the hot surface, fuelling unbending actuation, and helping the LCA recover to its initial position (state_1'). Due to the existence of motion inertia, the LCA continues waddling to the leftmost position (state_3). In this condition, the force bearing point of bracing force shifts to the left of the gravity force and the dynamic thermal equilibrium-induced thermo-mechanical actuation once again changes the film's center of gravity. Consequently, the LCA rotates to the reverse side. In this way, one cycle of the waddling actuation is achieved and the self-locked negative feedback loop sustains such oscillatory motions without changing the external stimulus. Compared with bilayer structure with light-driven oscillatory motions induced by the self-shadowing effect,[5a,24] both the triggering mechanisms are owing to the dynamic heat transfer and shape morphing induced nonequilibrium. The difference lies in whether the initial circumstance is equilibrium. In our case, the equilibrium symmetric external field triggering the LCA waddling calls for higher sensitivities of the actuator.

According to the simplified physical model described in Text S5 (Supporting Information), the frequency of the self-sustained waddling actuation will be affected by the mass, the height of geometry center, and the relative position of centroid center and geometry center. The latter two are highly related to the shape of LCA. Irregular oscillation occurs when the surface temperature is further increased, making the LCA roll over in an arch-bridge shape (Movie S8, Supporting Information). For instance, when $T = 95$ °C, γ of the LCA increases to 0.7 and the height of gravity center rises to 4.8 mm, which becomes greater than that of the geometry center (4.1 mm), thus causing the LCA to tip over after several tumbling cycles. A larger amplitude of 15.0 mm and a smaller oscillatory frequency of 1.0 Hz are obtained compared to 92 °C (Figure S18, Supporting Information), verifying the above theory.

2.4. LCA-Based Active Optical and Photonic Applications

By taking advantage of the light modulation capability of optically anisotropic LCs,[13c,25] we use LCAs to perform programmable self-sustained optical functionalities. Here we introduce a binary-phase grating structure with an alternative homogeneous LC structure and a twisted nematic LC structure into the right arm of the LCA by photopatterning (**Figure 4**a).[13c,26] Grating period d is designed to be 80 µm. A 2D beam steering system is proposed comprising only two components: the structured LCA and a commercial linearly polarized laser device (Figure 4b). To achieve better diffraction, the laser beam is carefully adjusted to only strike into the structured arm of LCA, i.e., right arm, by setting a slight deviation from the plane of the U-shaped LC ribbon. The incident polarization is parallel to the homogeneous alignment (Figure 4a). In this case, the Mauguin condition[27] (described in Text S6, Supporting Information) is satisfied, enabling the guiding control of outgoing polarization following the LC director distribution at the rear surface.

At $T = 90$ °C, the structured arm is highly lifted and nearly vertical to the laser propagation, suggesting a nearly normal incidence. Accordingly, a typical diffraction pattern is recorded comprising of a linear array of equally-spaced diffraction orders (Figure 4c). With the decrease of T, the bending deformation attenuates, leading to an increased incident angle θ_i. In this case, conical diffraction occurs with the propagating diffraction orders lying on the surface of a cone, giving rise to an angular separation of non-paraxial diffraction orders spreading in an arc shape. Factor θ_y, defined as the angle of diffraction spots deviating from the *x*-axis, is introduced here to characterize the steering capability of LCA in *y* direction. When T decreases from 90 to 40 °C, the bending degree φ linearly decreases from 81.5° to 6.6° (Figure 2d), thus θ_i is changed from 8.5° to 83.4° (Figure S19, Supporting Information). A typical conical diffraction pattern at 65 °C is presented in Figure 4c with $\theta_i = 49°$. The relationship between θ_y and θ_i is further provided in Figure 4d. $\theta_{y\_max} = 14.4°$ is achieved for the 24th-order diffraction spot at $\theta_i = 70°$. The 2D steering capability can be further enhanced by fabricating gratings with smaller periods (e.g., $d = 25$ µm, results in Figure S20, Supporting Information) according to the theory of conical diffraction.[28] Thus, by engineering the thermal field, we achieve robust, programmable 2D beam steering. The dynamic range can be encoded in both the microstructure and the macroscopic bending.

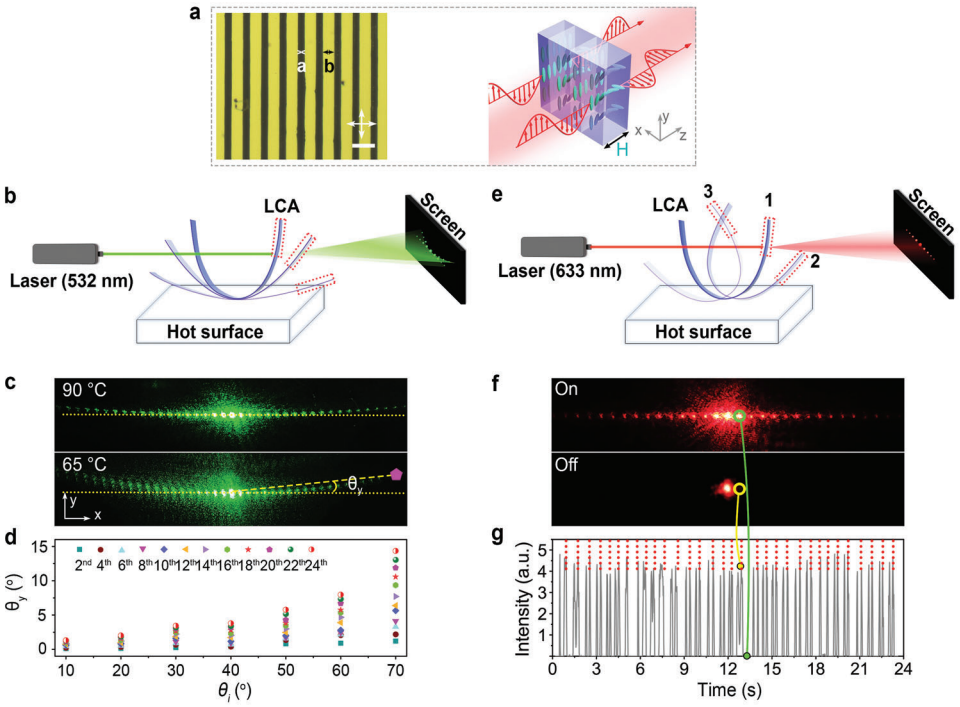

Figure 4. Programmable self-sustained thermo-mechanical-optical actuation. a) POM texture of the binary phase grating with alternatively changed homogeneous and twisted LC orientations; $a = 30$ µm and $b = 50$ µm (left). Schematic illustration of the binary phase grating with linearly polarized incident light (right). Scale bar: 100 µm. b) Schematic illustration of dynamic 2D beam steering based on an LCA partially with a binary phase grating (in the red dashed box). c) Diffraction patterns at $T = 65$ °C and $T = 90$ °C. The wavelength of the incident laser beam is 532 nm. d) Relationship between θ_y and θ_i for diffraction spots of different orders. e) Schematic illustration of self-sustained beam steering based on an LCA partial with a binary phase grating (in the red dashed box). f) On-off diffraction patterns. g) Time-dependent switching of the light intensity of 1st order. The red dashed lines represent the secondary periodicity of the time-dependent light diffraction. The wavelength of the incident laser beam is 632.8 nm.

In addition, the self-sustained waddling oscillations can be utilized in autonomous light modulation systems (Figure 4e). The right arm of LCA is fabricated with a grating structure, which oscillates from the neutral (position_1) to the rightmost (position_2), leftmost (position_3), and then back to the neutral position (position_1) during the periodic self-sustained waddling actuation. By elaborately adjusting the height of laser incidence (Figure S21, Supporting Information), we achieve diffraction when the LC ribbon is at neutral position_1 but non-diffraction when swinging to the rightmost position_2 or leftmost position_3 (Figure 4f), depending on whether the structured region of LCA is illuminated. Thereby, repeated self-regulating switching between on/off diffractions is attained as shown in Figure 4g. Time-dependent light intensity of diffraction with secondary periodicity ($P_2 = P_1$) occurs when the laser incidence is slightly deviated from the center of the microstructure region (Figure 4g). This phenomenon can be further exploited in autonomous beam steering systems with special periodicity. Further enciphering different structures spatially and sequentially on the arms may bring in abundant active optical functions including dynamic information encryptions.

Besides dynamic optical functionalities, we demonstrate active photonic applications based on LCAs. With one surface unidirectionally photoaligned ($\alpha = 0$) and the other space-variant photoaligned ($\alpha = \theta + \pi/4$, where θ is the azimuthal angle, **Figure 5**a), the LCA is endowed with the ability to produce special light fields based on the achromatic polarization-guiding effect. Corresponding POM texture is displayed in Figure 5b. A linearly polarized Gaussian beam is utilized normally incident to the structured arm when the actuator is at its neutral position. The incident polarization is parallel to the LC director on the homogeneously aligned front surface (Figure 5b). Then the propagating polarization chases the twisting of LC directors, yielding the output polarization following the local LC director distribution of the rear substrate. Consequently, whirlwind-like vector beams are generated (Figure 5c). Detections are carried out by inserting an analyzer after the actuator (Figure 5d). Thus, the autonomous self-sustained switching between the Gaussian beam and vector beam is realized.

Additionally, we offer the autonomous self-governing switching of focusing/defocusing performance by patterning a Fresnel lens phase structure ($\alpha = -\frac{\pi}{\lambda}(\sqrt{f^2 + r^2} - f)$, where λ is the wavelength, f is the focal length, and r is the radial distance), substituting for $\alpha = \theta + \pi/4$. Corresponding POM texture and the optical path for the focus/defocus switching are shown in Figure 5e and Figure S22 (Supporting Information), respectively. As a result, the conditions of exiting structured light at the focal plane are shown in Figure 5f, presenting focusing effect of left-handed circular polarized light (out_LCP), defocusing effect of right-handed circular polarized light (out_RCP), and the output light mixed with both focusing and defocusing components (out_LP). Hence, a platform for abundant active photonic

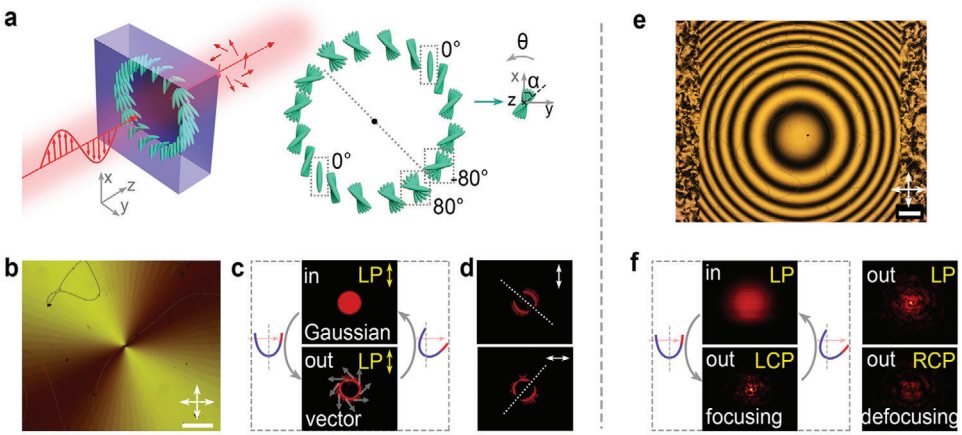

Figure 5. Autonomous active photonic functions enabled by LCAs. a) Schematic illustration of space-variant structured LCA with the incident light linearly polarized (left); Top view of LC director distribution of the spatially variant LCA structure (right). b) POM image of space-variant structured LCA. Scale bar: 250 μm. c) Switching of gaussian/vector beams during the actuator waddling. Yellow arrows indicate the incident polarization. d) Detection of vector beams with a linear polarizer. The polarization direction is indicated by white arrows. e) POM image of Fresnel-lens-structured LCA. Scale bar: 250 μm. f) Switching of defocusing/focusing beams during the waddling actuation. The incident and outgoing polarization states are indicated in the top right corner. The wavelength of the incident laser beam is 632.8 nm.

applications with programmable autonomous functionalities can be rationally expected.

3. Discussions and Conclusion

So far, we have demonstrated programmable bending actuation and autonomous self-sustained waddling oscillations for active optical and photonic functionalities. Monolithic twisted nematic LC ribbons with excellent thermal responsiveness are adopted instead of using bilayer configurations with different elastic moduli. The polymerized LC film with large-area ordered twisted structures of ≈1330 mm^2 can be tailored into more than 20 LC ribbons. These offer the feasibility of efficient fabrication. The drastic macroscopic bending deformation originates from the inherent symmetry-breaking chiral orientational structure of LC directors, revealing tremendous possibility in microstructure design. By harvesting easily-accessible thermal energy, the shape morphologies and self-initiated dynamics of LC ribbons can be artificially engineered, enabling intriguing flapping, sit-ups training, and penguin-like waddling motions. These actions can be exploited to dynamically modulate the light field with unique intelligent self-sustained optical/photonic functions by coupling the spatially periodic (static) microstructure of LCs and the temporally self-regulating (dynamic) locomotion of the actuator. Such function provides unique opportunities for self-sustained optical alarming and beam steering systems, optically visual sensing devices to perceive warning temperatures, and special laser processing avoiding photothermal-induced damage. By taking advantage of the high-resolution and arbitrary surface-pattern engineering of the photoalignment technique, more structured LCAs with various 3D architectures and high-quality optical functionalities can be rationally anticipated. Thus, it provides an important proof of principle for programmable spatial-temporal self-sustaining mechanical-optical systems. Besides macroscopic bending, we also achieve spring and helicoid deformations by cutting the thin film at different angles relative to the alignment directions (Figure S23, Supporting Information). The above dynamic motions could be activated in multiple scenarios, e.g., in vehicle or on asbestos net (Figure S24 and Movie S9, Supporting Information).

To summarize, we achieved various active optical applications based on soft smart LCAs with autonomous self-sustained thermo-mechanical-optical actuations. First, programmable thermo-mechanical bending and "sit-up" actuations are detailly investigated at the macroscopic scale. Second, higher temperature leads to ceaseless self-initiating, self-propelling, and self-sustaining "penguin-like waddling" oscillations along with a periodic self-feedback fluctuation of thermal distribution within the film. Finally, by exploiting both the microstructured elastic and optical anisotropies of LCs, programmed 2D beam steering and active modulations of special light fields are demonstrated, indicating an excellent platform not only for devising agile mechanical execution devices but also developing intelligent optical robotic systems. This work may inspire various soft automatic machinery with unique elastic properties and advanced optical functions, and provides an important proof of principle for autonomous active optical and photonic functionalities based on soft, smart, self-sustained LCAs.

Supporting Information

Supporting Information is available from the Wiley Online Library or from the author.

Acknowledgements

R.Z. and L.M. contributed equally to this work. The authors are indebted to Dr. Z. Man for her kind assistance with the microscopic observation. This work was funded by the National Key Research and Development Program of China (Nos. 2021YFA1202000 and 2022YFA1405000), the National Natural Science Foundation of China (No. 52003115), the Natural Science Foundation of Jiangsu Province, Major Project (No.

BK20212004), the Natural Science Foundation of Jiangsu Province (No. BK20200320). L.-L.Ma gratefully acknowledges the support of Xiaomi Young Scholar program.

Conflict of Interest

The authors declare no conflict of interest.

Data Availability Statement

The data that support the findings of this study are available from the corresponding author upon reasonable request.

Keywords

liquid crystals, optical materials, photoalignment, polymers, self-sustained actuators

Received: February 1, 2023
Revised: April 26, 2023
Published online: May 30, 2023

[1] a) S. Palagi, P. Fischer, *Nat. Rev. Mater.* **2018**, *3*, 113; b) K. Y. Ma, P. Chirarattananon, S. B. Fuller, R. J. Wood, *Science* **2013**, *340*, 603; c) Y. Huang, H. K. Bisoyi, S. Huang, M. Wang, X. M. Chen, Z. Liu, H. Yang, Q. Li, *Angew. Chem., Int. Ed.* **2021**, *60*, 11247.

[2] A. S Gupta, *WIREs Nanomed. Nanobiotechnol.* **2017**, *9*, e1464.

[3] a) M. Yang, Y. Xu, X. Zhang, H. K. Bisoyi, P. Xue, Y. Yang, X. Yang, C. Valenzuela, Y. Chen, L. Wang, W. Feng, Q. Li, *Adv. Funct. Mater.* **2022**, *32*, 2201884; b) Y. Wang, M. Li, J. K. Chang, D. Aurelio, W. Li, B. J. Kim, J. H. Kim, M. Liscidini, J. A. Rogers, F. G. Omenetto, *Nat. Commun.* **2021**, *12*, 1651.

[4] a) M. Vatankhah-Varnosfaderani, A. N. Keith, Y. Cong, H. Liang, M. Rosenthal, M. Sztucki, C. Clair, S. Magonov, D. A. Ivanov, A. V. Dobrynin, S. S. Sheiko, *Science* **2018**, *359*, 1509; b) H. Kim, J. Choi, K. K. Kim, P. Won, S. Hong, S. H. Ko, *Nat. Commun.* **2021**, *12*, 4658.

[5] a) L. Yang, L. Chang, Y. Hu, M. Huang, Q. Ji, P. Lu, J. Liu, W. Chen, Y. Wu, *Adv. Funct. Mater.* **2020**, *30*, 1908842; b) Z. Hu, Y. Li, J. A. Lv, *Nat. Commun.* **2021**, *12*, 3211; c) R. Merindol, A. Walther, *Chem. Soc. Rev.* **2017**, *46*, 5588; d) R. Lan, J. Sun, C. Shen, R. Huang, Z. Zhang, L. Zhang, L. Wang, H. Yang, *Adv. Mater.* **2020**, *32*, 1906319.

[6] T. M. Griffin, R. Kram, *Nature* **2000**, *408*, 929.

[7] a) D. Lentink, *Nature* **2013**, *498*, 306; b) P. Suomalainen, S. Sarajas, *Nature* **1951**, *168*, 211; c) J. E. Molloy, V. Kyrtatas, J. C. Sparrow, D. C. S. White, *Nature* **1987**, *328*, 449.

[8] X. Q. Wang, C. F. Tan, K. H. Chan, X. Lu, L. Zhu, S. W. Kim, G. W. Ho, *Nat. Commun.* **2018**, *9*, 3438.

[9] a) H. Zeng, O. M. Wani, P. Wasylczyk, R. Kaczmarek, A. Priimagi, *Adv. Mater.* **2017**, *29*, 1701814; b) Y. S. Zhang, A. Khademhosseini, *Science* **2017**, *356*, eaaf3627; c) W. Pang, S. Xu, J. Wu, R. Bo, T. Jin, Y. Xiao, Z. Liu, F. Zhang, X. Cheng, K. Bai, H. Song, Z. Xue, L. Wen, Y. Zhang, *Proc. Natl. Acad. Sci. U.S.A.* **2022**, *119*, e2215028119; d) Z. Xue, T. Jin, S. Xu, K. Bai, Q. He, F. Zhang, X. Cheng, Z. Ji, W. Pang, Z. Shen, H. Song, Y. Shuai, Y. Zhang, *Sci. Adv.* **2022**, *8*, eabm6922.

[10] L. Yu, H. Yu, *ACS Appl. Mater. Interfaces* **2015**, *7*, 3834.

[11] X. Xu, M. Tan, B. Corcoran, J. Wu, A. Boes, T. G. Nguyen, S. T. Chu, B. E. Little, D. G. Hicks, R. Morandotti, A. Mitchell, D. J. Moss, *Nature* **2021**, *589*, 44.

[12] a) L. L. Ma, C. Liu, S. B. Wu, P. Chen, Q. M. Chen, J. X. Qian, S. J. Ge, Y. H. Wu, W. Hu, Y. Q. Lu, *Sci. Adv.* **2021**, *7*, eabh3505; b) H. K. Bisoyi, Q. Li, *Chem. Rev.* **2022**, *122*, 4887.

[13] a) R. S. Zola, H. K. Bisoyi, H. Wang, A. M. Urbas, T. J. Bunning, Q. Li, *Adv. Mater.* **2019**, *31*, 1806172; b) X. Zhuang, W. Zhang, K. Wang, Y. Gu, Y. An, X. Zhang, J. Gu, D. Luo, J. Han, W. Zhang, *Light Sci Appl* **2023**, *12*, 14; c) P. Chen, L. L. Ma, W. Duan, J. Chen, S. J. Ge, Z. H. Zhu, M. J. Tang, R. Xu, W. Gao, T. Li, W. Hu, Y. Q. Lu, *Adv. Mater.* **2018**, *30*, 1705865; d) J. Xiong, Q. Yang, Y. Li, S. T. Wu, *Light Sci Appl* **2022**, *11*, 54; e) L.-L. Ma, S.-S. Li, W.-S. Li, W. Ji, B. Luo, Z.-G. Zheng, Z.-P. Cai, V. Chigrinov, Y.-Q. Lu, W. Hu, L.-J. Chen, *Adv. Opt. Mater.* **2015**, *3*, 1691.

[14] a) S. U. Kim, Y. J. Lee, J. Liu, D. S. Kim, H. Wang, S. Yang, *Nat. Mater.* **2022**, *21*, 41; b) Q. He, Z. Wang, Y. Wang, A. Minori, M. T. Tolley, S. Cai, *Sci. Adv.* **2019**, *5*, eaax5746.

[15] a) G. Babakhanova, H. Yu, I. Chaganava, Q. H. Wei, P. Shiller, O. D. Lavrentovich, *ACS Appl. Mater. Interfaces* **2019**, *11*, 15007; b) T. H. Ware, M. E. McConney, J. J. Wie, V. P. Tondiglia, T. J. White, *Science* **2015**, *347*, 982; c) M. O. Saed, C. P. Ambulo, H. Kim, R. De, V. Raval, K. Searles, D. A. Siddiqui, J. M. O. Cue, M. C. Stefan, M. R. Shankar, T. H. Ware, *Adv. Funct. Mater.* **2018**, *29*, 1806412.

[16] a) Y. Liu, B. Xu, S. Sun, J. Wei, L. Wu, Y. Yu, *Adv. Mater.* **2017**, *29*, 1604792; b) J. Zhang, Y. Guo, W. Hu, M. Sitti, *Adv. Mater.* **2021**, *33*, 2100336; c) A. H. Gelebart, D. J Mulder, M. Varga, A. Konya, G. Vantomme, E. W. Meijer, R. L. B. Selinger, D. J. Broer, *Nature* **2017**, *546*, 632; d) W. Feng, D. J. Broer, D. Liu, *Adv. Mater.* **2018**, *30*, 1704970; e) J. A. H. P. Sol, L. G. Smits, A. P. H. J. Schenning, M. G. Debije, *Adv. Funct. Mater.* **2022**, *32*, 2201766.

[17] J. Zhang, Y. Guo, W. Hu, R. H. Soon, Z. S. Davidson, M. Sitti, *Adv. Mater.* **2021**, *33*, 2006191.

[18] a) Y. Zhao, Y. Chi, Y. Hong, Y. Li, S. Yang, J. Yin, *Proc. Natl. Acad. Sci. U.S.A.* **2022**, *119*, e2200265119; b) F. Ge, Y. Zhao, *Chem. Sci.* **2017**, *8*, 6307.

[19] M. Pilz da Cunha, A. R. Peeketi, A. Ramgopal, R. K. Annabattula, A. Schenning, *ChemistryOpen* **2020**, *9*, 1149.

[20] Y. Li, Y. Liu, D. Luo, *Adv. Opt. Mater.* **2020**, *9*, 2001861.

[21] M. Pilz da Cunha, A. R. Peeketi, K. Mehta, D. J. Broer, R. K. Annabattula, A. Schenning, M. G. Debije, *Chem. Commun.* **2019**, *55*, 11029.

[22] J. Jeon, J.-C. Choi, H. Lee, W. Cho, K. Lee, J. G. Kim, J.-W. Lee, K.-I. Joo, M. Cho, H.-R. Kim, J. J. Wie, *Mater. Today* **2021**, *49*, 97.

[23] S. Tu, L. Xu, J. K. El-Demellawi, H. Liang, X. Xu, S. Lopatin, S. De Wolf, X. Zhang, H. N. Alshareef, *Nano Energy* **2020**, *77*, 105277.

[24] B. Zuo, M. Wang, B. P. Lin, H. Yang, *Nat. Commun.* **2019**, *10*, 4539.

[25] L. L. Ma, C. Y. Li, J. T. Pan, Y. E. Ji, C. Jiang, R. Zheng, Z. Y. Wang, Y. Wang, B. X. Li, Y. Q. Lu, *Light Sci Appl* **2022**, *11*, 270.

[26] L. L. Ma, M. J. Tang, W. Hu, Z. Q. Cui, S. J. Ge, P. Chen, L. J. Chen, H. Qian, L. F. Chi, Y. Q. Lu, *Adv. Mater.* **2017**, *29*, 1606671.

[27] S. T. Wu, D. K. Yang, *Fundamentals of liquid crystal devices*, John Wiley & Sons, West Sussex, England, UK **2014**.

[28] J. E. Harvey, C. L. Vernold, *Appl. Opt.* **1998**, *37*, 8158.

